https://doi.org/10.5194/egusphere-2024-8
Preprint. Discussion started: 20 February 2024

Co- and postseismic subaquatic evidence for prehistoric fault activity near Coyhaique, Aysén Region, Chile

Morgan Vervoort[1], Katleen Wils[1], Kris Vanneste[2], Roberto Urrutia[3], Mario Pino[4], Catherine Kissel[5], Marc De Batist[1], Maarten Van Daele[1]

[1]Renard Centre of Marine Geology (RCMG), Department of Geology, Ghent University, 9000 Ghent, Belgium
[2]Royal Observatory of Belgium, 1180 Brussels, Belgium
[3]Centro EULA, Universidad de Concepción, Casilla 160-C, Concepción, Chile
[4]Instituto de Ciencias de la Tierra, Universidad Austral de Chile, Casilla 567, Valdivia, Chile
[5]Laboratoire des Sciences du Climat et de l'Environnement/IPSL, CEA/CNRS/UVSQ, Université Paris-Saclay, 91198 Gif-sur-Yvette, France

Correspondence to: Morgan Vervoort (Morgan.Vervoort@UGent.be)

Abstract. Chilean Patagonia is confronted with several geohazards due to its tectonic setting, i.e., the presence of a subduction zone and numerous fault zones (e.g. the Liquiñe-Ofqui Fault Zone). This region has therefore been the subject of numerous paleoseismological studies. However, this study reveals that the seismic hazard is not limited to these large tectonic structures by identifying past fault activity near Coyhaique in the Aysén Region. Mass wasting deposits in Lago Pollux, a lake located ca. 15 km SW of this region's capital, were identified through analysis of reflection-seismic data and was linked to a simultaneous event recorded in nearby Lago Castor. Furthermore, a coeval ~50 year-long catchment response was identified in Aysén Fjord based on the multiproxy analysis of a portion of a sediment core. Assuming that this widely recognized event was triggered by an earthquake, ground-motion modelling was applied to derive the most likely magnitude and source fault. The model showed that an earthquake rupture along a local fault, in the vicinity of Lago Pollux and Lago Castor, with a magnitude of 5.6-6.8, is the most likely scenario.

1 Introduction

Lake and fjord sediments represent continuous archives of natural hazards, such as earthquakes or volcanic eruptions, in a variety of tectonic settings (e.g., Moernaut, 2020; Sabatier et al., 2022; St.-Onge et al., 2004). Seismic shaking in such basins can cause widespread and coeval mass wasting and/or surficial sediment remobilization, recorded as mass transport deposits (MTDs) and/or turbidites (e.g., Adams, 1990; Howarth et al., 2014; Kremer et al., 2017). The presence of such coeval deposits forms the basis of the synchronicity criterion (Adams, 1990; Schnellmann et al., 2002), which is typically invoked to infer an earthquake as most likely source-mechanism. Numerous studies have successfully applied this approach for the reconstruction of a regional seismic history (e.g., Kremer et al., 2017; Moernaut et al., 2007, 2014; Praet et al., 2017; Schnellmann et al., 2002; Strasser et al., 2007; Wilhelm et al., 2016; Wils et al., 2020). Apart from the coseismic effects of earthquake shaking, a long-term increased sediment yield may also occur in lacustrine or fjord basins due to earthquake-induced landslides and perturbations in their catchment. Several recent studies evidenced such postseismic enhanced sediment flux (e.g., Avşar et al., 2014; Howarth et al., 2012, 2014). Lake and fjord sediments may thus preserve both coseismic and postseismic imprints and are therefore valuable archives of past seismic activity.

Numerous paleoseismological studies have been conducted in Chile due to its active tectonic setting (e.g., Moernaut et al., 2007, 2014; Piret et al., 2018; Van Daele et al., 2015, 2019; Wils et al., 2018, 2020). In a recent study of the sedimentary infill of Lago Castor, located in the Andean mountains (45.6°S, 71.8°W), Van Daele et al. (2016) identified a turbidite (dated between 4300 and 4450 cal yrs BP), associated to multiple MTDs, suggesting it was triggered by an earthquake (~synchronicity criterion), although the causative fault remains unclear. The subduction zone is likely too far away to be able to cause significant shaking in the area, as suggested by the fact that no damage was reported during the 1960 M_w 9.5 Valdivia

https://doi.org/10.5194/egusphere-2024-8
Preprint. Discussion started: 20 February 2024

earthquake (Lazo, 2008). A more established source of seismic hazard in the region is the Liquiñe-Ofqui Fault Zone (LOFZ) (Hervé, 1976), although the closest branch of this fault system is located about 50 km from the lake. Some small, local fault traces have been identified closer to the lake, but their activity is largely unknown (De La Cruz et al., 2003; Sernageomin, 2003). In any case, the possibility of an earthquake occurring and generating strong seismic shaking close to Coyhaique, the district capital, is important for the hazard and risk assessment of the area, thus justifying further research into this past event. In this respect, we studied the seismic stratigraphy of Lago Pollux (about 3 km southwest of Lago Castor) in order to reveal its sedimentary history and achieve a correlation with the sedimentary infill of Lago Castor. Identification of the presence or absence of synchronous large-scale mass-wasting in this nearby lake would significantly improve our understanding of the size and impact of this presumed paleo-earthquake. We also analyzed a section of a sediment core retrieved from inner Aysén Fjord, located at the same latitude but closer to the megathrust, for comparison with the Lago Pollux and Lago Castor records. In Aysén Fjord, multiple sedimentary imprints of both megathrust and crustal earthquakes along the LOFZ were already identified (Wils et al., 2018; 2020). By combining the sedimentary data in these two lakes and one fjord with ground-motion modelling we aim to identify the most likely location and magnitude of this ~4400 cal yrs BP paleo-earthquake.

2 Study area

2.1 Regional setting

Lago Pollux is located in southern Chile, in the Aysén Region on the eastern side of the Patagonian Andes, close to the Argentinian border (Figure 1a). Chilean Patagonia has a humid climate with low seasonality and a west-to-east precipitation gradient resulting from the dominant Southern Westerly Winds (SWW or southern westerlies) (Gilli et al., 2005; Henry, 2005). The vegetation surrounding the lake is mainly pastureland, covered by fallen and burnt logs resulting from deforestation of the subantarctic *Nothofagus pumilio* forest (Markgraf et al., 2007). Lago Pollux has a surface area of 9.06 km^2 and is situated ~680 m above sea level (m asl), on a plateau where also Lago Castor and Lago Thompson are located (Figure 1b). Their catchment mainly contains Cretaceous rocks and Cenozoïc volcanoclastics (De La Cruz et al., 2003; Sernageomin, 2003), and the surrounding hills reach heights of over 1000 m. The main inflow for Lago Pollux comes from Lago Castor and Lago Thompson, which are situated around 20 m and 70 m higher, respectively. These two lakes have no major inflow apart from some surrounding creeks. Lago Pollux then drains towards Lago Frío, located about 150 m lower at the base of the plateau, via a small river at its central western side. Finally, Lago Frío drains via the Río Simpson, eventually flowing through Río Aysén into Aysén Fjord, located on the western side of the Patagonian Andes (Figure 1a, c). The geology in the area surrounding Aysén Fjord is dominated by igneous rocks such as granites, (grano-)diorites and tonalites of the North Patagonian Batholith. However, an important part of the catchment and that of the feeding rivers (i.e., Río Cuervo, Río Condor River, Río Mañihuales and Río Simpson) is composed of basaltic to rhyolitic Quaternary volcanic centers (De La Cruz et al., 2003; Sernageomin, 2003).

2.2 Volcanotectonic setting

The Aysén Region is seismically active, owing to its location close to the Peru-Chile subduction trench, where the oceanic Nazca Plate obliquely subducts below a continental portion of the South American Plate. The oblique subduction additionally results in the presence of a large crustal strike-slip fault system, the Liquiñe-Ofqui Fault Zone (LOFZ; Figure 1a), of which one of the major fault strands crosses Aysén Fjord (Legrand et al., 2011; Métois et al., 2012). Between about 44 and 46°S, east of the main LOFZ fault strands and Aysén Fjord, two major north-northeast trending faults can be distinguished: the Azul Tigre and Río Mañihuales Faults (Figure 1a) (Thomson, 2002). However, none of these major tectonic structures reach towards

https://doi.org/10.5194/egusphere-2024-8
Preprint. Discussion started: 20 February 2024

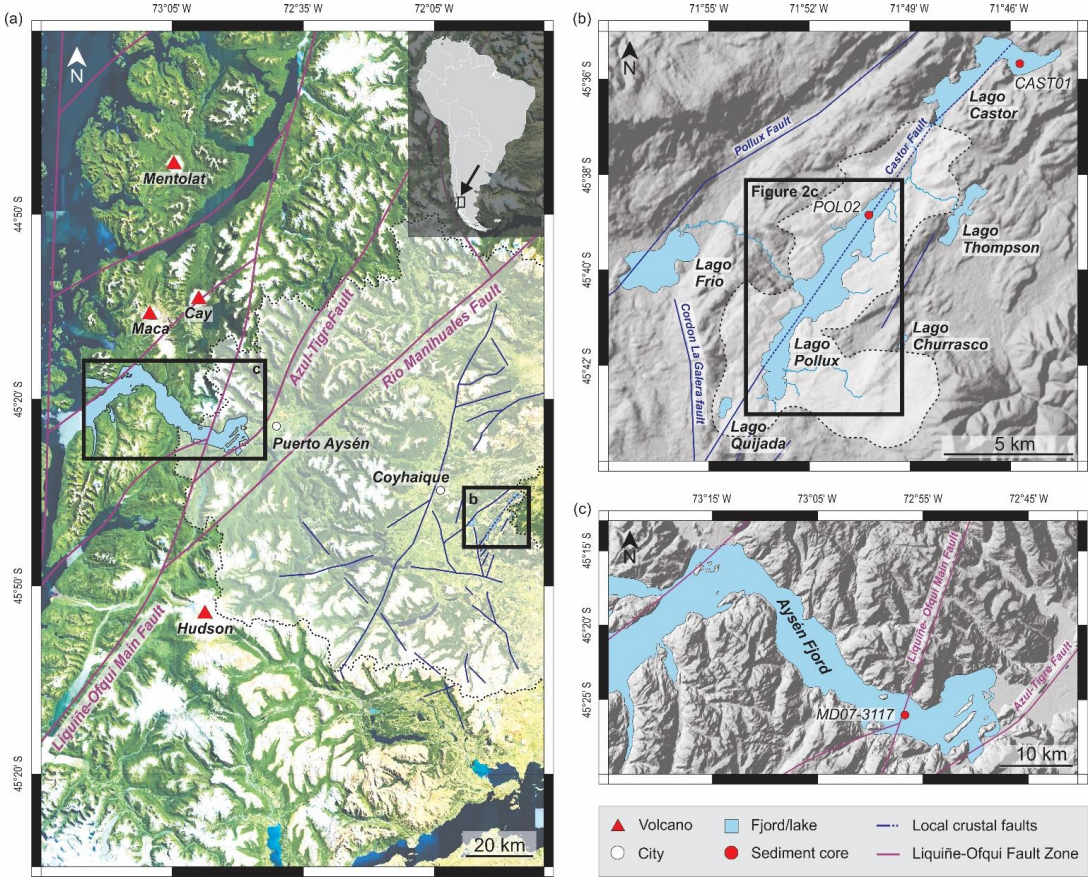

Figure 1. (a) World imagery map (Esri, 2022) of the study are. The Liquine-Ofqui Fault Zone (LOFZ) and smaller faults surrounding the city of Coyhaique are indicated (De La Cruz et al., 2003), as well as the catchment area of Aysén Fjord (light shaded zone). (b) Shaded NASA Shuttle Radar Topography Mission Global 1 arc (SRTMGL1N) terrain data (NASA JPL, 2013) of the area surrounding Lago Pollux, including Lago Castor, Lago Frio, Lago Thompson, Lago Churrasco, Lago Quijada and local faults. The catchment area of Lago Pollux (light shaded zone) and major rivers surrounding Lago Pollux (light blue), as well as the location of short sediment cores in both Lago Pollux and Lago castor are indicated. (c) SRTMGL1N terrain data (NASA JPL, 2013) of the inner Aysén Fjord area with retrieved sediment core MD07-3117 indicated.

the area of Lago Castor and Lago Pollux, where only multiple local smaller crustal faults have been mapped (Figure 1a, b; De La Cruz et al., 2003; Sernageomin, 2003). Apart from seismic activity, the presence of a subduction zone also results in an active volcanic arc. From ~33°S to 46°S, the volcanic arc is referred to as the Southern Volcanic Zone (SVZ), characterized by complex volcano-tectonic interactions (Cembrano and Lara, 2009). An illustration of this interaction is the 2007 seismic swarm affecting Aysén Fjord (Agurto et al., 2012; Legrand et al., 2011). At first, the swarm was thought to have a solely tectonic origin (Cembrano et al., 2007), but it was later confirmed to have a fluid-driven source mechanism as well. In this case, both magma and water, from Aysén Fjord itself or hydrothermal vents therein, may have interacted to generate the seismic swarm (Legrand et al., 2011). Some of the active volcanoes in the Aysén Region are the Mentolat, Cay, Macá and Hudson volcanoes (Figure 1a) (Naranjo and Stern, 2004; Stern, 2004). The Hudson Volcano is the southernmost and most active volcano of the SVZ (Naranjo and Stern, 2004; Weller et al., 2018). Due to the prevailing winds, most of its eruptions had ashes dispersed in an eastward direction (Naranjo and Stern, 1998), towards the Lago Castor and Pollux area, where the resulting tephra deposits can thus serve as regional markers. The three largest Holocene eruptions of the Hudson Volcano are H1, H2 and H3 with ages of 8.50-8.01 cal yr BP, 4.09-3.61 cal yr BP and 1991 AD, respectively (Naranjo and Stern, 1998, 2004; Weller et al., 2014), all of which have been identified in the sedimentary infill of Aysén Fjord (Wils et al., 2018; 2020). An even larger eruption, with an estimated tephra volume of more than 20 km^3, has been described by Weller et al. (2014).

https://doi.org/10.5194/egusphere-2024-8
Preprint. Discussion started: 20 February 2024

This event, called Ho, has a pre-Holocene age of 17.30-17.44 cal yr BP and its tephra has been identified in Lago Churrasco and Lago Quijada, located less than 3 km east and 1.5 km south-west of Lago Pollux, respectively (Figure 1a, b). In addition to the Ho tephra, also the H2 tephra has been identified in both of these lakes (Moreno et al., 2019). Also in Lago Castor, both the Ho and H2 deposits were identified, alongside an additional 52 tephra deposits (Van Daele et al., 2016).

3 Material and methods

3.1 Lago Pollux and Lago Castor

A geophysical survey with both a CENTIPEDE sparker and GEOPULSE pinger source system, from the Renard Centre of Marine Geology (RCMG – Ghent University), resulting in (very) high resolution sub-bottom seismic profiles, was conducted in December 2009 on Lago Pollux. The sparker produces a broad-spectrum seismic signal (0.4-1.5 kHz), with a mean frequency of ~1.3 kHz, resulting in a maximum vertical resolution of ~0.5 m. A single-channel streamer with 10 hydrophones was used as a receiver The pinger operates at a mean frequency of ~3.5 kHz, resulting in a slightly higher vertical resolution of ~0.2 m. The survey was conducted in conjunction with a similar geophysical survey on neighboring Lago Castor. In addition, short sediment cores (< 1 m) were taken in both lakes (Fig. 1b), as well as a long sediment core (>15 m)in Lago Castor. The short gravity cores were split, imaged and their magnetic susceptibility was measured with a Bartington MS2E point sensor at a 2.5 mm step size. The long Lago Castor core has a composite length of 15.4 m and was described and interpreted by Van Daele et al. (2016). The sedimentary history of Lago Pollux is presumed to be similar to that of Lago Castor due to their proximity and hydrographic connection (Figure 1b). The seismic data of Lago Pollux was interpreted using the IHS Markit Kingdom Software (version 2019), allowing for identification of several seismic units of which the thickness was estimated based on the corresponding acoustic velocities from Lago Castor (Van Daele et al., 2016). A bathymetric map was produced by gridding of the lake floor reflector picks using Surfer (Golden Software). An acoustic velocity of 1450 m/s was assumed for water of 10 °C (Del Grosso, 1974), which is about the average water temperature in Lago Pollux, as determined by a CTD profile at the time of the seismic survey.

3.2 Aysén Fjord

A Calypso sediment core, MD07-3117, of 21.14 m length was retrieved from inner Aysén Fjord during the PACHIDERME cruise on board of the RV *Marion Dufresne* in February 2007. Wils et al. (2018, 2020) studied the core in detail to create an event record of earthquakes and volcanic eruptions for the Aysén Fjord region. For that purpose, the archive half was scanned with the Ghent University Hospital medical computed tomography (CT) scanner (Siemens; SOMATOM Definition Flash; Siemens AG) at ~0.2 mm resolution in x and y directions, and a 0.6 mm z-resolution. VGStudio 3.2 was used for visualization. The present study focusses on sections VIII and IX of the core (9.5-12 m depth), which has an age range (Wils et al., 2020) covering that of the mass-wasting event identified in the sedimentary infill of Lago Castor (Van Daele et al., 2016). Both sections were logged with the Geotek Multi Sensor Core Logger (MSCL) of Ghent University to obtain high-resolution spectrophotometric (Konica Minolta CM-2600d) and MS data at a 2 mm interval. The acquired color reflectance data was used to calculate the normalized relative absorption band area between 400 and 560 nm ($nRABA_{400\text{-}560}$) and reflectance ratio between 590 and 690 nm (R_{590}/R_{690}). The former has been used as a proxy for total organic carbon (TOC) content (Vandekerkhove et al., 2020) and is calculated by the following formula (Rein and Sirocko, 2002):

$$nRABA_{400-560} = \left[\left(\frac{R_{590}}{R_{400}}\right) + \cdots + \left(\frac{R_{590}}{R_{560}}\right)\right] / R_{mean}$$

in which R_{590} is the reflectance at 590 nm, R_{400} at 400 nm and R_{560} at 560 nm. R_{mean} is the average reflectance of all measured reflectance values (360 – 740 nm). The R_{590}/R_{690} index is a proxy for the presence of illite, biotite and chlorite and is calculated by dividing the reflectance value at 590 nm (R_{590}) by the reflectance value at 690 nm (R_{690}) (Trachsel et al., 2010).

https://doi.org/10.5194/egusphere-2024-8
Preprint. Discussion started: 20 February 2024

Two sets, each with a total of 35 samples (taken at a 1 cm interval), were taken in section IX for grain-size analysis and estimation of organic matter content. This includes four samples in a previously-identified turbidite that has been related to a megathrust earthquake (Wils et al., 2020). For each sample, grain-size analysis was performed with a Malvern Mastersizer 3000 after chemical pre-treatment to remove organic matter, calcium carbonate and biogenic silica (procedure after Van Daele et al., 2016). The grain-size data was subsequently unmixed into different grain-size populations or end members (EM), using the MATLAB-based toolbox AnalySize (Paterson and Heslop, 2015). Additionally, loss-on-ignition (LOI) was performed to estimate the organic matter content (Heiri et al., 2001). The samples were first dried for 24 hours at 105°C (LOI_{105}), after which they were heated to 550°C for four hours (LOI_{550}). The LOI_{550} values were calculated using the dry sediment weight (LOI_{105}).

Ten samples were selected to determine the elemental (C and N) and stable isotope ($\delta^{13}C$) composition in order to identify the source – terrestrial or marine – of the sedimentary organic matter (Carneiro et al., 2021). The optimal sample weight was calculated based on the LOI_{550} values. The samples were placed in silver capsules and treated with 25 µl of sulfurous acid (H_2SO_3, 6-8%) to remove any inorganic carbon. The organic geochemical analysis was carried out by the Isotope Bioscience Laboratory (ISOFYS) of Ghent University with the Elemental Analyzer – Isotope Ratio Mass Spectrometer-I (EA-IRMS-I ANCA-GSL), interfaced with a 20-22 IRMS, SerCon. The standard deviation on the $\delta^{13}C$ measurements is < 0.6 ‰ on the Vienna Pee Dee Belemnite (VPDB) scale. Normalization on VPDB scale was done using two soil references with certified $\delta^{13}C$ values (-22.69 ± 0.04 ‰ and -28.85 ± 0.1 ‰).

3.3 Ground-motion modelling

Our analysis of the sedimentary infill of Lago Pollux and Aysén Fjord in the period around 4400 cal yrs BP, allow us to identify the presence or absence of sedimentary deposits that can be related to the major mass-wasting event identified in Lago Castor. For coeval deposits over a large area, an earthquake-related triggering mechanism is generally assumed. In that case, the presence or absence of coeval deposits can be used as positive or negative evidence for seismic shaking, respectively. To generate coseismic deposits (positive evidence), a minimum level of shaking is required, depending on the type of deposits. For major onshore landslides and rockfalls, a shaking intensity of VII½ or higher is generally required (e.g., Keefer, 1984; Serva et al., 2016), and is confirmed by the observations following the 2007 Mw6.2 earthquake in Aysén Fjord (Naranjo et al., 2009; Sepúlveda et al., 2010). Subaquatic mass-movements can occur with intensities of VI½ and higher (e.g., Moernaut et al., 2014; Monecke et al., 2004; Van Daele et al., 2015; Wilhelm et al., 2016). Delta failures require the least intense shaking, and can occur when intensity V½ is exceeded (e.g., Moernaut et al., 2014; Van Daele et al., 2020). The absence of such deposits (negative evidence) implies that these threshold levels of ground shaking were probably not exceeded. To accommodate for variability in preconditioning factors, such as slope angle or availability of sediment (e.g., Bernhardt et al., 2015; Molenaar et al., 2019; Strasser et al., 2007) that may affect the susceptibility to slope failure, we added ½ intensity unit for the threshold value associated to negative evidence (Kremer et al., 2017; Vanneste et al., 2018). In other words, the absence of onshore landslides implies that intensities of VIII were not reached, as exceeding this value is assumed to always result in onshore mass wasting.

The most likely source location and magnitude for the considered earthquake can be estimated using the observed set of positive and negative earthquake evidence, in combination with their respective intensity thresholds, and by applying the probabilistic ground-motion modelling methodology developed by Vanneste et al. (2018). This requires the use of an intensity prediction equation (IPE), which provides the shaking intensity for any site in the vicinity of an earthquake with known magnitude and location. By calculating the intensities caused by a range of earthquakes with different magnitudes and locations in a grid that comprises the study sites, the probability for each of these potential earthquakes to have caused the observed pattern of positive and negative evidence can thus be calculated. For this study, the IPE developed by Bakun and Wentworth (1997) was chosen, as it has proven to adequately represent the seismic shaking observed during crustal earthquakes in the

https://doi.org/10.5194/egusphere-2024-8
Preprint. Discussion started: 20 February 2024

Aysén Region (Vanneste et al., 2018). However, as the BakunWentworth1997 IPE does not have an explicit uncertainty term, we arbitrarily considered a 1σ standard deviation of 0.4 on the calculated intensities (Vanneste et al., 2018). In our analysis, we only considered crustal earthquakes with magnitudes ranging between 4.5 and 7.5, as lower magnitudes are unlikely to cause sufficient shaking for mass wasting to occur and higher magnitudes are uncommon in a crustal tectonic setting. Each of these potential ruptures was first modelled with a strike of 30°, dip of 80°, and rake of 180°, which corresponds to the mean orientation of the right-lateral strike slip faults in the LOFZ. Earthquake depth does not affect modelling outcomes as the BakunWentworth1997 IPE only takes into account epicentral distances. This is reasonable since faults in the LOFZ often have a surface trace and do not extend to great depths. Most earthquakes in the 2007 Aysén seismic swarm, for example, did not nucleate at depths larger than 10 km (Legrand et al., 2011). These results were subsequently refined by considering known faults in the region (Figure 1a) rather than a grid of potential earthquake ruptures with identical, average values for strike, dip and rake.

4 Results

4.1 Bathymetry

Based on its bathymetry (Figure 2c), Lago Pollux can be divided into three subbasins: a deep northern subbasin, a deep central subbasin and a shallow southern subbasin (NSB, CSB and SSB, respectively). The NSB and SSB are elongated, while the CSB is wider and more circular. The deepest part of the lake, with a water depth of 56 m, is situated in the NSB. The transition from the NSB to the CSB is marked by a clear shallower part, incised by a small channel of about 40-45 m deep. The CSB is again deeper with a maximum depth of about 52 m. The SSB is a shallow subbasin, reaching depths of maximum 25-30 m in its northern and central part and shallowing to ≤ 5-10 m in its southernmost part. This shallow environment leads to low or even no penetration of the acoustic waves. The transition between the CSB and SSB is a shallow, small area of maximum 35-40 m deep. In a bay along the eastern shore of the NSB and CSB, depths of ≤ 5 to maximum 15 m are reached before evolving into the steeper slopes that flank the deeper basins. The slopes along the western shore of the NSB are steep. At the main outflow (western shore of the CSB) and the northern inflow (northern shore of the NSB), we observe a more gentle slope.

4.2 Geophysical data analysis of Lago Pollux

Five different seismic-stratigraphic units overlying the bedrock were identified on the seismic profiles of Lago Pollux (Figure 2a,b).

Unit 1 is the lowermost seismic unit with a very variable thickness, ranging from ~24 m to less than 1 m. This unit only occurs locally and is mainly restricted to the deepest parts of the basin, filling local depressions. However, it is also present on bedrock highs throughout the NSB and CSB. It has a chaotic to transparent seismic facies.

Unit 2 is the thickest sedimentary unit and is mainly observed in the NSB, where it has a maximum thickness of ~45 m in the central part, thinning towards ~36 m in the southern part. It is only sporadically present in the CSB with varying thickness of

https://doi.org/10.5194/egusphere-2024-8
Preprint. Discussion started: 20 February 2024

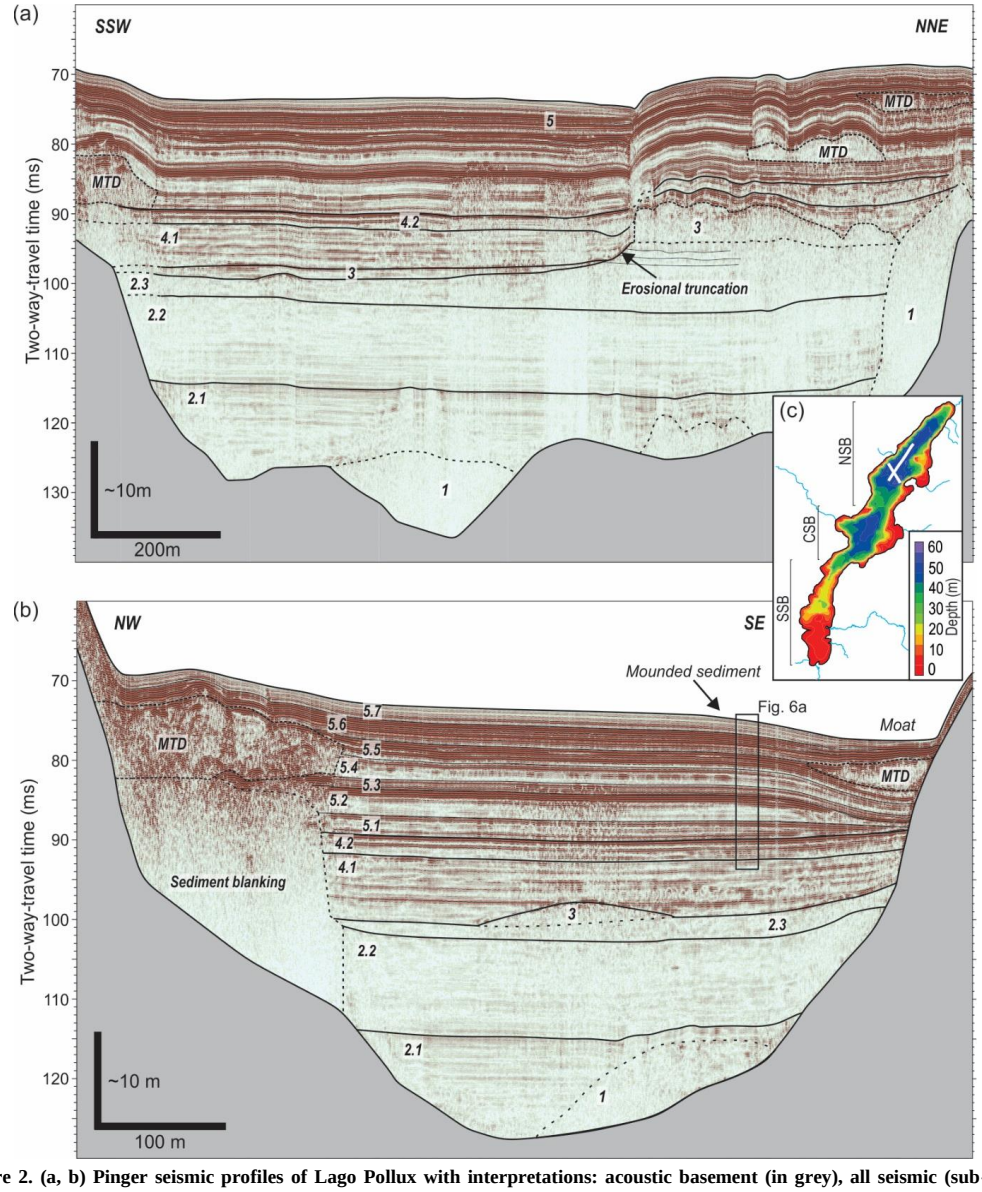

Figure 2. (a, b) Pinger seismic profiles of Lago Pollux with interpretations: acoustic basement (in grey), all seismic (sub-)units (numbers) and mass transport deposits (MTDs) are indicated. (c) Bathymetry of Lago Pollux with indication of subbasins (NSB: northern subbasin, CSB: central subbasin, SSB: southern subbasin) and location of the two pinger seismic profiles (white lines).

20 to 40 m. This unit is characterized by continuous, (sub-)parallel and generally low-amplitude reflections. It shows a ponded geometry, filling up the deep subbasins, and does not drape the slopes. Three subunits can be identified based on subtle differences in reflection amplitude. The first subunit (Unit 2.1) shows generally higher-amplitude reflections compared to Unit 2.2 and 2.3. The seismic reflectors of Unit 2.1 are onlapping the acoustic basement or Unit 1, when present. At the top of Unit 2.3, erosional truncations can be observed at both the western and eastern slopes in the NSB and CSB (Fig. 2a), making the top-boundary an unconformity.

Unit 3 is a distinctive unit in which two different seismic facies can be identified: a chaotic to transparent facies and a hummocky facies. The chaotic-transparent facies is present in patches in the northern and central parts of the NSB and only sporadically observed in the CSB. Both the upper and lower boundaries form a clear unconformity with the surrounding seismic units. The hummocky facies, consisting of small higher-amplitude, discontinuous reflections, can only be observed in the

https://doi.org/10.5194/egusphere-2024-8
Preprint. Discussion started: 20 February 2024

southern part of the NSB, which is the deepest part of the paleobasin (top of Unit 2). It has a maximum thickness of ~3 m and, in contrast to the chaotic facies, it shows a conformable upper and lower boundary.

Unit 4 is typically thicker in the NSB compared to the CSB (up to ~23 m and ~16 m thick, respectively). However, unlike the underlying seismic units, it is observed throughout the entire basin. Its seismic facies is composed of subparallel to parallel continuous reflections. The unit is subdivided into two subunits, separated by a high-amplitude reflection, which is in turn covered by a chaotic to transparent facies with ponding geometry (Figure 2a). The whole unit shows an onlapping basal contact with Unit 2 and Unit 3 (when present). As a result, Unit 4.1 is more basin-focused than Unit 4.2, which is more widely distributed across the lake.

Unit 5 is the uppermost seismic unit with a thickness of ~11 m in the deepest parts, showing continuously stratified seismic reflections that drape the previous unit. Towards the south-eastern slopes, the seismic reflections show a convergent facies, leading to a thinner sediment package (up to 6-8 m). Several thin subunits, seven in total, are identified throughout the basin based on differences in their reflection amplitude (Fig. 2b). Additionally, multiple chaotic deposits can be identified in Subunits 5.1, 5.2 and 5.5. All chaotic deposits in Unit 5.1 and Unit 5.2 are located in the central and northern part of the NSB, except one which is found at the transition of the CSB to the SSB. Most deposits are located at the foot of the slope, with the exception of one deposit that is positioned towards the deeper areas of the central part of the NSB. The chaotic deposits in Unit 5.5 are mostly located along the western slope in the central and southern part of the NSB and the entire CSB. However, different deposits are identified along the eastern slope of the NSB and one at the eastern slope of the central CSB. The deposits along the eastern and western slopes show a very different seismic facies and morphology. Deposits along the western slope have a very chaotic facies and display successive frontal thrusts. Furthermore, seismic blanking of the underlying strata can occur (Fig. 2b). On the other hand, the deposits along the eastern slopes show a more transparent and less chaotic facies (Fig. 2b). Additionally, they form relatively thin, lens-shaped sediment bodies located at the foot of the slope, thinning towards the central part of the subbasin. At the same horizon (top of Unit 5.5) in the deepest part of the basin, thin deposits with a transparent facies and ponding geometry can be identified (Figure 2a, b).

4.3 Lago Pollux and Lago Castor lithology

4.3.1 Short cores

The short sediment cores (~60 cm), POL02 and CAST01 from Lago Pollux and Lago Castor, respectively, consist of laminated light to dark brown diatomaceous mud (Figure 6b). We identify intercalations of multiple coarser and darker layers and interpret them as tephra layers. Overall, a low MS signal is recorded for the laminated mud (Figure 6b), but four thicker tephra layers of 0.5 - 1.5 cm are marked by peaks in the MS values. Throughout the cores, and especially at the base of the cores, multiple smaller peaks are observed, indicating various smaller tephra beds. A correlation between both cores, and thus both lakes, is made based on the tephra layers and corresponding MS signal.

4.3.2 Lago Castor U5.2 and 5.5 turbidite

The Lago Castor long sediment core consists mostly of grey and light to dark brown laminated mud and is described by Van Daele et al. (2016). Three turbidites were identified, of which two occur in the top 7.5 m of the core: in Unit 5.2 and 5.5. The turbidite in Unit 5.5 is located ~15 cm below a 20 cm thick tephra layer, interpreted by Van Daele et al. (2016) as the H2 Hudson Volcano tephra layer. This turbidite has a very similar sedimentary composition as the background sediment and corresponds to what Van Daele et al. (2015)describe as type 1 lacustrine turbidites (LT1), resulting from sediment remobilization on hemipelagic slopes. Multiple MTDs were identified on that same horizon in the seismic profiles from Lago Castor (Van Daele et al., 2016).

https://doi.org/10.5194/egusphere-2024-8
Preprint. Discussion started: 20 February 2024

4.4 Sedimentological analyses of Aysén Fjord

4.4.1 Color and reflectance spectroscopy

The MD07-3117 core consists mostly of light to dark brown mud and is partly bioturbated (Wils et al., 2018). Section IX of the core (Figure 3) clearly shows around 11.02 m depth a darker (lower brightness, L*) layer with a strong increase in radiodensity and $nRABA_{400-560}$ values. Wils et al. (2020) identified this layer as a turbidite related to a megathrust earthquake. Additionally, a lighter-colored (increased brightness, L*) layer of about ~10 cm thick is present between ~11.15 and ~11.23 m, which is also marked by an increase in radiodensity, albeit less pronounced, and lower $nRABA_{400-560}$ values compared to the background sediment. Furthermore, the R_{590}/R_{690} index shows higher values compared to those in the remainder of the studied core section, even higher than those observed in the turbidite. This layer was not recognized as an event deposit by Wils et al. (2020). Below this interval, at 11.26 and 11.31 m throughs in $nRABA_{400-560}$ values, corresponding to peaks in R_{590}/R_{690} index and L*, can be explained by reworking of the sediments from the lighter-colored layer through bioturbation, and are thus post-depositional in nature. A correlation plot between the $nRABA_{400-560}$ and R_{590}/R_{690} values clearly shows three different clusters: one corresponding to the background sediment samples, one to the turbidite sediments and one to the lighter-colored layer sediments (Figure 4a), indicating variations in source material.

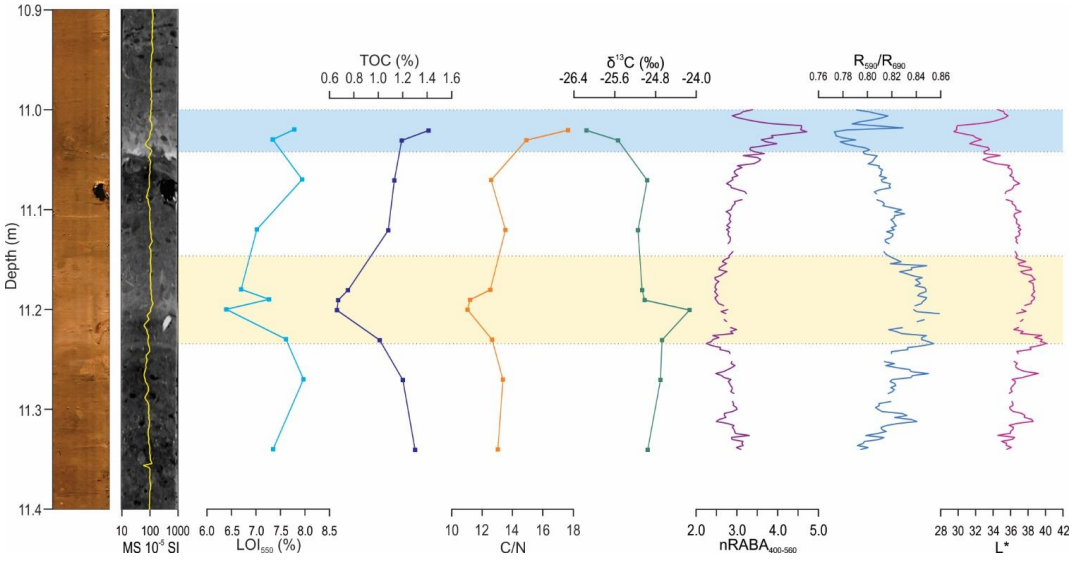

Figure 3. Digital image and CT-scan of a portion (section IX, 10.9-11.4 m) of the MD07-3117 sediment core from inner Aysén Fjord, with bulk organic geochemistry and spectrophotometry data (from left to right): organic matter content (LOI550), total organic carbon content (TOC), carbon-nitrogen ratio (C/N), 13-carbon isotope fraction (δ 13C), normalized relative absorption band area between 400-560 nm (nRABA400-560), reflectance ratio between 590 and 690 nm (R590/R690) and brightness (L*). The turbidite (11.0-11.04 m) identified by Wils et al. (2020) and the lighter-colored layer (11.14-11.24 m) are indicated by blue and yellow bands, respectively. Gaps in the spectrophotometry data are due to previous sampling (holes) in the core.

4.4.2 Bulk organic geochemistry

Throughout the studied core section, LOI_{550} values are rather low and less than 8 %. The lowest values occur in the lighter-colored layer, while the turbidite shows higher values compared to the background sediment. A similar trend can also be seen in the TOC and C/N results (Figure 3). In the lighter-colored layer, TOC values only reach about 0.66 % and the C/N ratio is about 11. For the background sediment, the TOC content varies between 1.08-1.30 % and the C/N ratio between 13.0-13.5. The turbidite has a markedly higher TOC content of 1.41 % and a higher C/N ratio of 17.6. The opposite trend can be seen in $\delta^{13}C$ values, where values of -26.2 ‰ are reached at the base of the turbidite and -24.1 ‰ in the lighter-colored layer. However, these samples were at the limit of the measurement capability of the instrumentation, resulting in an uncertain accuracy of the

https://doi.org/10.5194/egusphere-2024-8
Preprint. Discussion started: 20 February 2024

reported $\delta^{13}C$. Lastly, a positive correlation is present between the TOC content, and LOI_{550} and $nRABA_{400\text{-}560}$ values (Figure 4b). Generally it is assumed that the LOI_{550} is two times the TOC-content, as typically ~50 % of organic matter is composed of organic carbon (Pribyl, 2010). Here, the slope of the linear regression between the LOI_{550} and TOC values shows that ~72 wt% of the organic matter is organic carbon, while the intercept indicates that LOI_{550} overestimates the organic matter content with ~6 %. This means other components are also present, such as water in clays and oxides, explaining the apparent higher LOI_{550} values. This is also reflected in the $nRABA_{400\text{-}560}$ and R_{590}/R_{690} correlation plot (Figure 4a), where the $nRABA_{400\text{-}560}$ is a proxy for the TOC. As the R_{590}/R_{690} values are a proxy for clastic material, it can be concluded that for the same organic matter content, the lighter-colored layer contains more clastic components compared to the background sediment and turbidite (Figure 4a).

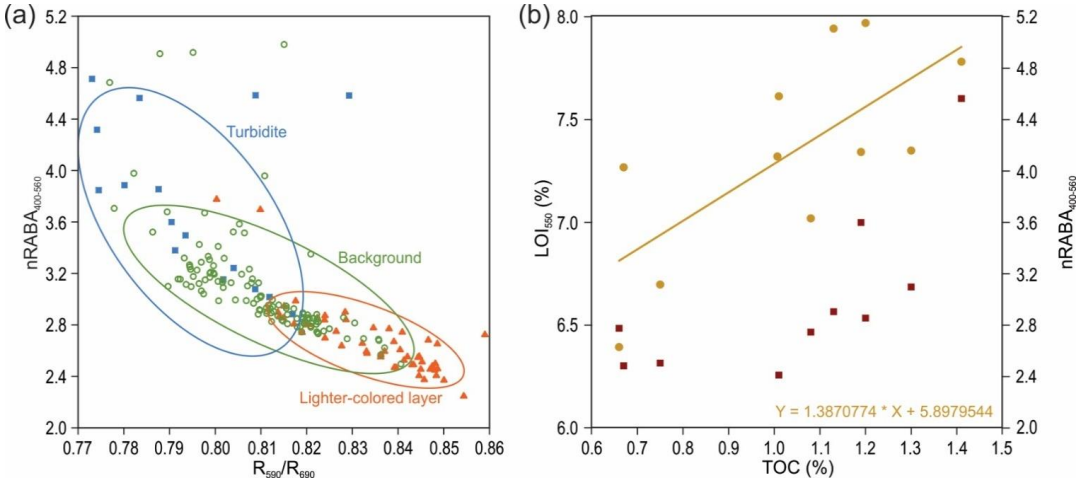

Figure 4. (a) Correlation of the normalized relative absorption band area between 400-560 nm (nRABA400-560) and reflectance ratio between 590 and 690 nm (R590/R690) showing three distinct clusters: background sediment (green circles), turbidite (blue squares) and lightered-colored layer (orange triangles). (b) Correlation between total organic carbon (TOC) content with nRABA400-560 (red squares) and organic matter content (LOI550) (yellow circles).

4.4.3 Grain size

According to the Udden-Wentworth classification, sediments in the studied core section can be described as silt, ranging from very fine silt in the lighter-colored layer to fine silt in the background sedimentation and medium silt at the base of the turbidite (Figure 5a). Throughout this core section, the sorting values are rather low and generally below ~3 µm. However, two peaks of poorer sorting up to ~5 µm can be seen at the base of the lighter-colored interval. In the turbidite, a slight increase in geometric sorting values is seen from the base towards the tail, indicating the coarse-grained base is slightly better sorted then the finer sediments of the tail (Figure 5b). Three different EMs ($R^2 = 0.9912$) can be identified from the grain-size distributions of our 35 samples, two of which correspond well with the two finest EMs defined by Wils et al. (2020) for the complete MD07-3117 core (Figure 5c, d). The first population (EM0) consists of very fine material with a mode of 2.94 µm and is most abundant in the lighter-colored interval (Figure 5c). The second (EM1) shows a larger grain-size mode of 5.57 µm and corresponds to the background EM described by Wils et al. (2020). Lastly, an end-member with a coarser mode of 19.95 µm is identified, corresponding with the finest turbidite EM identified by Wils et al. (2020), and is thus also mostly present in the turbidite (Figure 5c).

https://doi.org/10.5194/egusphere-2024-8
Preprint. Discussion started: 20 February 2024

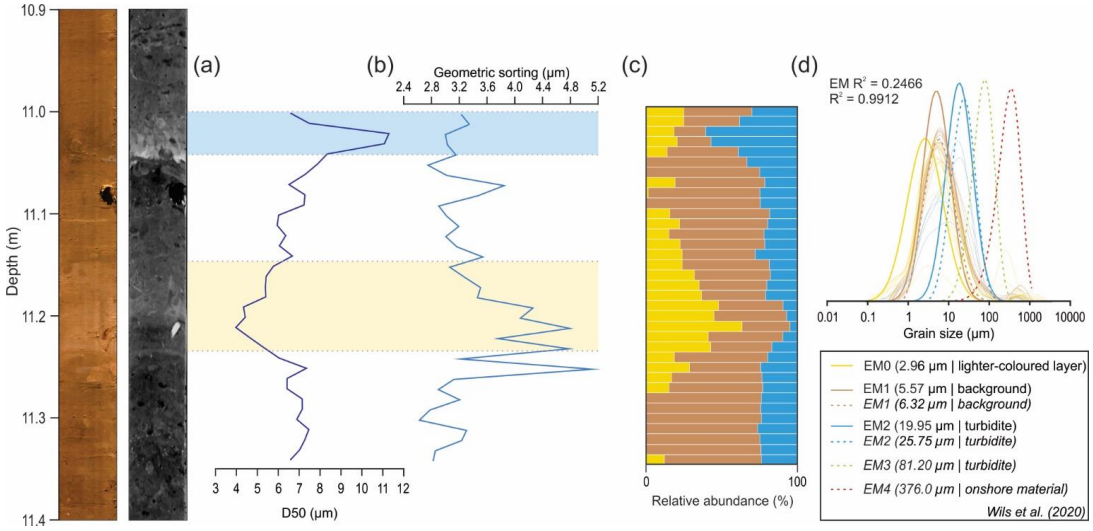

Figure 5. Digital image and CT-scan of a portion (10.9-11.4 m) of the MD07-3117 sediment core from inner Aysén Fjord, with grain-size data including (a) D50 values and (b) geometric sorting. (c) Relative abundance plot of the different end members identified in the portion of the MD07-3117 sediment core (EM0, EM1, EM2). (d) Plotted end member distributions of this study (full lines) with end member distributions from Wils et al. (2020) (dotted lines).

5 Discussion

5.1 Sedimentary history of Lago Pollux

A similar seismic stratigraphy as Lago Castor is expected in Lago Pollux due to their proximity and similar geomorphological position (both lakes are located on the same plateau). The units will be described and correlated to Lago Castor based on the interpretations of Van Daele et al. (2016).

Based on similarities with the lowermost units of sedimentary infills of other glacial lakes and fjords (e.g., Heirman et al., 2011, 2012; Ndiaye et al., 2014; Van Rensbergen et al., 1998), the chaotic deposits of Unit 1 in Lago Pollux can be interpreted as glacial till deposits (Fig. 2a, b). Moreover, similar deposits were identified in Lago Castor, where they date back to MIS2 or MIS4 (Van Daele et al., 2016). This indicates that a glacial cover was present over Lago Castor and Lago Pollux during these late glacial times.

During deposition of Unit 2, the sedimentary environment likely evolved to that of a sub- or proglacial lake characterized by more regular, glaciolacustrine sedimentation (e.g., Heirman et al., 2011; Ndiaye et al., 2014; Van Rensbergen et al., 1998; Figure 2a, b). This is also observed in Lago Castor, where a varved proglacial sedimentary unit was identified (Van Daele et al., 2016). Unit 2 shows the same seismic characteristics and geometry in Lago Pollux and Lago Castor, allowing to interpret them as varved sediments as well. In Lago Castor Unit 2 is much thicker (up to 78 m) compared to Lago Pollux, possibly indicating an earlier onset in sedimentation. Additionally, a thinning of the unit is observed from the NSB to the CSB in Lago Pollux, thus suggesting a deglaciation from NE to SW, in line with the general model for deglaciation of the Patagonian Ice Sheet (Davies et al., 2020).

The dispersed character of Unit 3, in combination with its transparent to chaotic facies, is distinctive for mass transport deposits (MTDs) (e.g. Moernaut and De Batist, 2011; Praet et al., 2017; Wils et al., 2018). This widespread mass wasting likely occurred around the same time as an erosional event, which is marked by the erosional features found at the top of Unit 2.3 (Figure 2a). Van Daele et al. (2016) also identified such an erosional event at the same seismic-stratigraphic level in Lago Castor, which was interpreted as erosion during lake level lowstand after a rapid drainage around > ~20 kyr BP. The model proposed by Van Daele et al. (2016) predicts a drainage of Lago Castor through the narrow northern and central Lago Pollux subbasins. In Lago

https://doi.org/10.5194/egusphere-2024-8
Preprint. Discussion started: 20 February 2024

Pollux, the observed erosion may thus be related to the discharge event itself, where the exposed slopes subsequently or coevally failed, producing the observed MTDs.

After the event, the very low lake level rose gradually as shown by the ponding morphology and onlapping continuously-laminated seismic facies of Unit 4.1 (Figure 2a). Since deposition of Unit 4.2, sediments drape the entire lake floor and are no longer limited to the deeper parts of the basins. A similar trend was also found in Lago Castor (Van Daele et al., 2016). Furthermore, in both lakes, a discontinuous high-amplitude reflection can be identified within this seismic-stratigraphic unit, in Lago Pollux covered by a chaotic/transparent facies with a ponding geometry (Figure 2a). In Lago Castor, where it has a thickness of ~60 cm in the sediment core, this deposit is attributed to the presence of a volcanic ash layer that was identified in the sediment core and interpreted as the Ho Hudson Volcano tephra (Van Daele et al., 2016). Considering the proximity of both lakes and the dominant westerly wind directions (Gilli et al., 2005), the discontinuous high-amplitude reflections in both lakes are considered to be correlated and represent the base of the Ho tephra layer.

The most recent seismic-stratigraphic unit, Unit 5, in both Lago Pollux and Lago Castor shows draping and continuously laminated sediments, occasionally interrupted by MTDs (Figure 2a, b). The divergent seismic facies and the presence of moats at the SE flanks in Lago Pollux (Figure 2b) are also present in Lago Castor, where they are interpreted as sediment drifts linked to SWW activity since ~16.75 kyr BP (Van Daele et al., 2016). The seven subunits identified in Lago Castor are also seen in Lago Pollux (Figure 2b, 6a). Van Daele et al. (2016) related the high-amplitude reflections separating the subunits to the presence of tephra layers. Indeed, when comparing the short sediment cores from both lakes, representing the uppermost sediments of Unit 5.7, a very similar sedimentation can be seen, with an almost identical pattern of MS peaks, which represent the thin tephra layers (Figure 6b). As high-amplitude reflections correspond to tephra layers, it is not surprising that the subunits in Unit 5 correspond between both lakes. Apart from Ho, the most prominent tephra layer identified in the sedimentary infill of Lago Castor (top reflector of Unit 5.5) was interpreted as the H2 Hudson Volcano tephra deposit (Van Daele et al., 2016). Hence, this tephra deposit is likely responsible for the strong reflector draping the MTDs at the top of Unit 5.5 in Lago Pollux (Figure 2a, b, 6a).

As expected, analysis of the seismic and sediment core data shows that Lago Pollux and Lago Castor experienced a very similar sedimentary evolution.

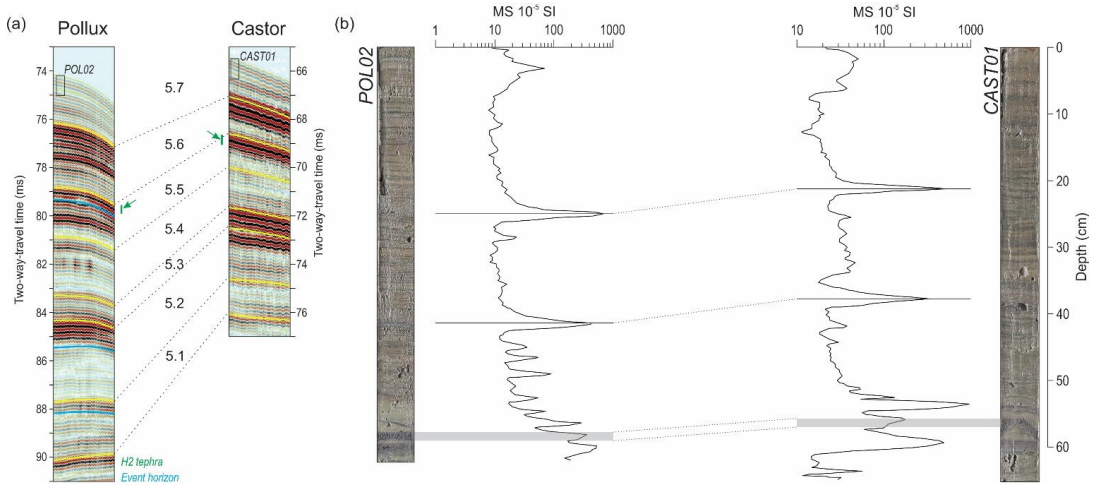

Figure 6. (a) Seismic section of Unit 5 showing all seven subunits identified on a pinger seismic profile in Lago Pollux (Fig. 2b) and Lago Castor (after Van Daele et al., 2016). (b) Correlation of two short cores from Lago Pollux (POL02) and Lago Castor (CAST01) with plotted MS data, showing two distinct peaks. At the base, a ~1.5 cm thick tephra in both cores is indicated in grey.

https://doi.org/10.5194/egusphere-2024-8
Preprint. Discussion started: 20 February 2024

5.2 Synchronous mass wasting and a catchment response

Towards the central part of the basin in Lago Pollux, the ponded, seismically transparent deposit associated with the MTDs of Unit 5.5 is interpreted as a turbidite (Figure 2a, b, 7). At the same seismic-stratigraphic horizon in Lago Castor, several MTDs were identified, correlating with a thin turbidite in the sediment core (Van Daele et al., 2016). We interpret that the presence of these event deposits with multiple MTDs at the same stratigraphic horizon (i.e. with 0.2 m accuracy) in these hydrologically open, neighboring lakes is not coincidental, and hence, that they represent the same event. According to the synchronicity criterium (Adams, 1990; Schnellmann et al., 2002), the observation of synchronous mass-wasting in two separate lakes points to a single, regional trigger mechanism for this event, most likely earthquake shaking. The event occurred before the H2 Hudson Volcano eruption, as the MTDs are covered by the associated tephra deposit. The age difference between the turbidite and H2 tephra in the sediment core from Lago Castor is ~350 years (Van Daele et al., 2016) (Figure 8), which is thus assumed to be identical in Lago Pollux. The H2 tephra deposit was also found in Aysén Fjord, albeit with a slightly older age range (Wils et al., 2018, 2020) (Figure 8), enabling a correlation between all three sedimentary records.

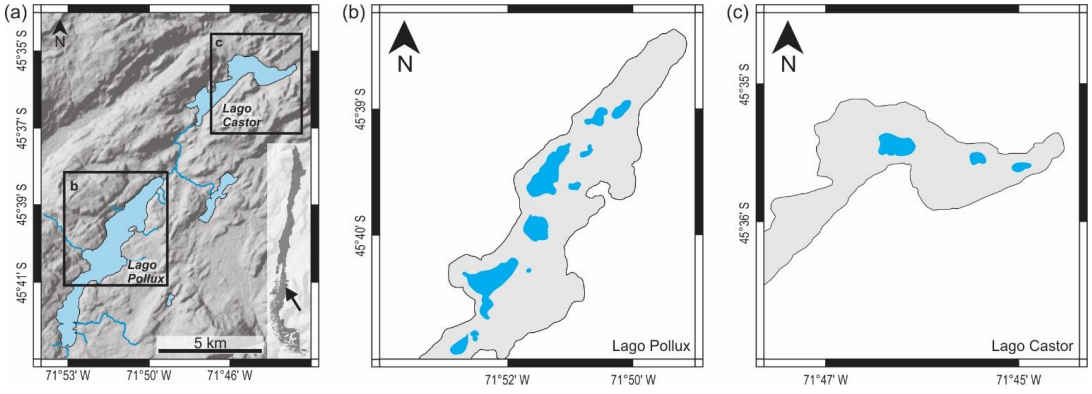

Figure 7. Spatial distribution of the mass transport deposits (MTDs) identified in Unit 5.5 under the H2 tephra deposit for both (a) Lago Pollux and (b) Lago Castor. Note that the distribution of MTDs in the southern part of Lago Pollux could not be mapped due to shallow bathymetry and limited seismic penetration, and that no MTDs were identified in the southwestern part of Lago Castor.

To verify whether the inferred earthquake responsible for mass wasting in Lago Castor and Lago Pollux also affected Aysén Fjord, the results of grain-size analysis, organic geochemistry and spectrophotometry measurements on the section of the core below the H2 deposit were analyzed. Three deposits appear distinctively different from the background sediment: two turbidites related to megathrust earthquakes by Wils et al. (2020), and the lighter-colored interval (Figure 3). While the absolute age of neither of these deposits matches with that of the turbidite in Lago Castor, the relative age difference between the base of lighter-colored interval and the H2 deposit (~385 years) is very similar to the age offset observed for the turbidite and H2 tephra in Lago Castor (Figure 8). This confirms that the observed mass-wasting in Lago Castor and Lago Pollux was not related to a megathrust earthquake (i.e., no MTDs or turbidite in Aysén Fjord), but rather to a local shaking event in the catchment of the Aysén Fjord. Moreover, this event seems to have resulted in lighter-colored sediment input in the fjord (Figure 8). This is interpreted as a catchment response signal: significant mass wasting in the Aysén Fjord catchment, consisting of volcanic rocky soils and low amounts of vegetation, could lead to a temporary increase in clastic sedimentation input. Indeed, an overall low organic matter content is observed in this finer-grained layer (Figure 3) as well as an increase in clastic material (Figure 4a). The apparent anomalously low C/N values in this catchment response (Figure 3) can be explained by decomposition processes of organic matter in the catchment soils. These processes comprise microbial immobilization of N-rich material accompanied by remineralization of C (Meyers and Ishiwatari, 1993; Shanahan et al., 2013). Furthermore, the andosol soils in the Aysén Region are already low in organic matter due to weathering processes on the hilly slopes (Ellies, 2000; Gut, 2008), explaining the overall low C/N (and TOC) values of the layer. The $\delta^{13}C$ values show an opposite trend, with higher values in the lighter-colored layer (Figure 3). This enrichment in $\delta^{13}C$ can also be explained by the decomposition processes of soil

https://doi.org/10.5194/egusphere-2024-8
Preprint. Discussion started: 20 February 2024

organic matter. In the CO_2 resulting from microbial respiration of soil organic matter, the lighter isotope of carbon (^{12}C) is preferred to be incorporated, leaving the heavier ^{13}C isotope behind (Shanahan et al., 2013). The long-distance, fluvial transport from the catchment area towards the depositional center in Aysén Fjord could further explain the finer grain-size trend observed in this layer (Figure 3). In this case, the increase in clastic sedimentation input lasted for a maximum of ~50 years (Figure 8). Such timeframe seems plausible because at present, 16 years after the 2007 Aysén M_w 6.2 earthquake, which caused multiple landslides in the Aysén Fjord area (Sepúlveda et al., 2010), not all of the then-exposed slopes have been re-vegetated; and increased erosion rates thus likely persist. If the earthquake epicenter was located more to the east (which is expected based on the observed combination of shaking imprints, and will later on be confirmed by ground-motion modelling) where the climate is drier, this process would be even slower.

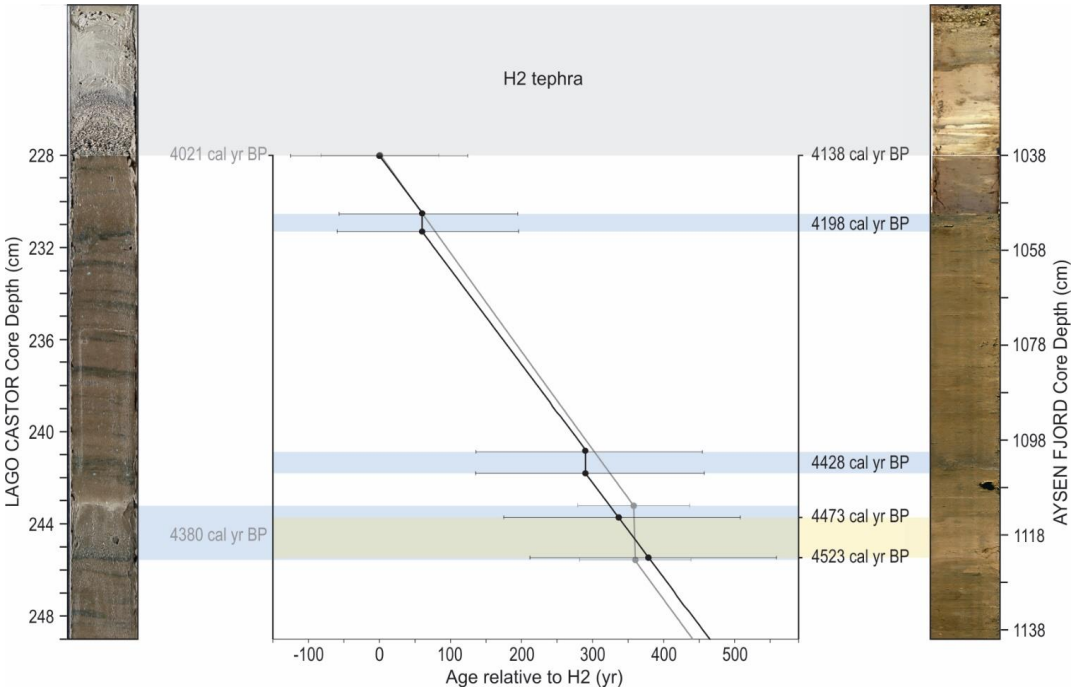

Figure 8. Correlation figure between the sediment core retrieved from Lago Castor (left) and Aysén Fjord (right) (core pictures not to original scale). The graph shows an age-depth model relative to the H2 Hudson Volcano tephra deposit (4.09-3.61 cal yr BP; Naranjo and Stern 1998; grey band). Turbidites in both cores are indicated by blue bands and the lighter-colored interval by a yellow band. The correlation shows an overlap between the deposition of the turbidite from Lago Castor and lighter-colored layer from Aysén Fjord.

5.3 Locating the earthquake source

For each of the study sites, the minimum and/or maximum intensity of seismic shaking is determined based on the sedimentary evidence (Table 1). In Lago Castor, all identified MTDs attributed to the earthquake ~4400 years ago are located along the lake slopes (Figure 7). These consist of hemipelagic sediments, and no post-seismic catchment response (pointing to onshore mass-wasting, cfr. Howarth et al., 2012) was identified (Figure 8). This implies that the shaking intensity at the time of the earthquake must thus have exceeded VI½ (i.e., threshold for failure of lateral lacustrine slopes covered with hemipelagic sediments), but remained well below VIII (i.e., threshold for onshore landslides in the catchment). In Lago Pollux, similar, albeit more widespread, MTDs are observed (Figure 7), but it is unclear whether these consist of hemipelagic sediment or rather originated onshore due to the lack of a sediment core. A minimum shaking intensity of VI½ must thus have been achieved, but a maximum threshold cannot confidently be assigned. Local shaking intensities in Aysén Fjord are considered

https://doi.org/10.5194/egusphere-2024-8
Preprint. Discussion started: 20 February 2024

not to have exceeded VI, as not even a failure of the Río Aysén delta could be identified, which would have resulted in a turbidite similar to those that have been related to megathrust earthquakes, (Wils et al., 2020).

Table 1: Overview of all earthquake evidence used as input for ground-motion modelling in all study sites

	Positive evidence	Negative evidence
Lago Castor	≥ VI½	< VIII
Lago Pollux	≥ VI½	/
Aysén Fjord	/	< VI
Río Aysén catchment	> VII½ in predefined area	/

However, the ~50 year period of enhanced sediment input (Figure 8) does indicate that a significant amount of landslides must have occurred in the Rio Aysén catchment. This provides an additional constraint for the ground-motion modelling, as intensities of VII½ must have been exceeded at least in a part of the Río Aysén catchment. The maximum size of the area affected by landslides during an earthquake increases with magnitude (Keefer, 1984; Rodríguez et al., 1999). This relationship also holds true for observations in the Aysén Fjord area following the 2007 M_W 6.2 earthquake (Sepúlveda et al., 2010), and can thus be used to estimate the area that would have been affected by landslides during the ~4400 cal yrs BP event. In general, no landslides can be observed for earthquakes with an M_W lower than 4, while an earthquake with M_W 8 results in a maximum affected area of about 100,000 km² (Keefer, 1984; Rodríguez et al., 1999). In practice, this implies that the entire Río Aysén catchment, with a size of about 13,000 km², could have been affected. Considering the ~50 year duration of increased sediment input in Aysén Fjord as a result of this earthquake, it is unlikely that onshore landslides occurred in an area smaller than 100 km². However, it is impossible to determine exactly what part of the catchment experienced high enough shaking to produce onshore landslides as this depends on a number of factors such as earthquake depth and geological site conditions, influencing the presence of slide-susceptible sites and seismic attenuation. Therefore, we test a range of areas varying between 100 and 10,000 km² (within the Río Aysén catchment) and use the minimum intensity threshold of VII½ to limit the range of possible

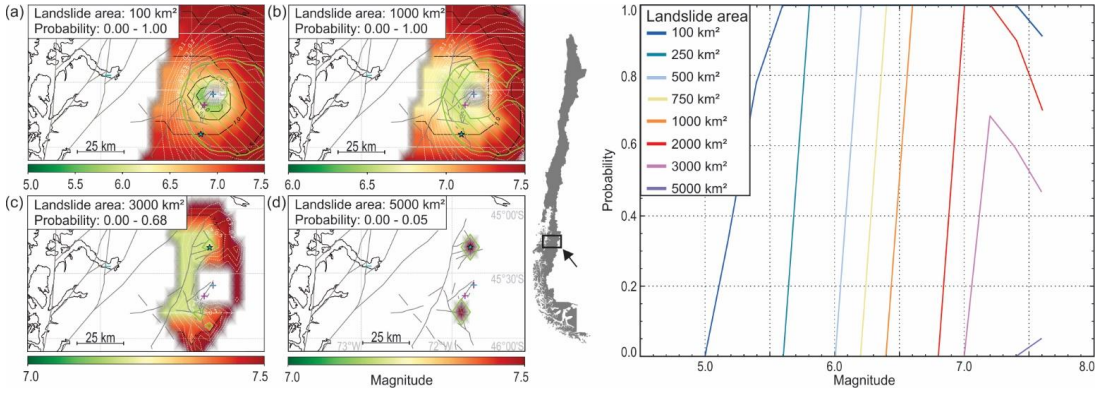

Figure 9. Left: Maps (location indicated on grey map of Chile) showing the area in which an earthquake could have caused the observed pattern of sedimentological imprints In Lago Pollux, Lago Castor and Aysén Fjord (positive and negative evidence), considering an area of 100 (a), 1000 (b), 3000 (c) and 5000 (d) km² that was affected by landslides. The magnitude with the highest probability at each location is given in a green-to-red color scale. White dashed lines correspond to the probability; green line and enclosed hatched area mark the region where the probability is less than 0.1 below the maximum probability, highlighting the most likely epicentral region (indicated by a star). Sites of positive (plus) and negative (minus) evidence are shown in semitransparent magenta and cyan colors, respectively. Note that sites with both positive and negative evidence show a bluish color. Right: The maximum probability of an earthquake in the study area (independent of its location) with a magnitude ranging between 5 and 7.6 to have caused the observed pattern of sedimentological imprints In Lago Pollux, Lago Castor and Aysén Fjord (positive and negative evidence), considering a range of minimum areas (100-5000 km²) in the Rio Aysén catchment that were affected by landslides.

https://doi.org/10.5194/egusphere-2024-8
Preprint. Discussion started: 20 February 2024

sources that are considered in the probabilistic method: earthquake ruptures that cannot produce this intensity of seismic shaking (based on forward application of the IPE) in a predefined minimum portion of the Río Aysén catchment are discarded. As expected, modelling results show that, for any of the predefined area values, the probabilities for a crustal fault to cause the considered combination of positive and negative evidence are zero for any earthquake in the western part of the catchment, close to Aysén Fjord (Figure 9), meaning that the earthquake must have occurred close to Lago Castor and Lago Pollux. This immediately rules out the potential for an LOFZ-rupture to have caused the observed mass-wasting, and indicates that a local earthquake must have occurred ~4400 years ago. Moreover, it is highly unlikely that this earthquake caused landslides over an area of 3000 km² or larger in the Río Aysén catchment, as probabilities then rapidly decrease to zero (Figure 9). For an area of 100 km², maximum probabilities can be observed for earthquakes with an M_W between 5.5 and 7.5. Probabilities remain high for areas of up to 2000 km², although the minimum earthquake magnitude then increases to 7.0. The considered landslide area thus mostly constrains the minimum magnitude required to result in the observed mass-wasting.

When taking into account the approximate fault traces in the area (Figure 10), reasonable probabilities (> 50%) are only obtained for areas around 1000 km² or smaller and for earthquakes with magnitudes below 7, regardless of the considered landslide area. This indicates that most of the faults are in an unfavorable location or not sufficiently long to produce the right range of shaking intensities at the study sites and simultaneously affect a large portion of the Río Aysén catchment. The minimum magnitude is again constrained by the size of the landslide area within the Río Aysén catchment, with an M_W of 5.6 for 100 km², increasing to 6.4 for 500 km² and 6.8 for 1000 km². For higher magnitudes, probabilities decrease significantly and the most likely responsible fault also shifts westward, away from Lago Castor and Lago Pollux and towards Coyhaique (Figure 10).

Earthquakes related to the subduction megathrust were not taken into account here, as these are considered too distant to cause significant shaking in the Lago Pollux area (Lazo, 2008). Furthermore, we also do not consider intraslab earthquakes, as Lago Pollux and Lago Castor are situated merely 30-40 km north of the slab window that results from the subduction of the Chile Ridge (Russo et al., 2010), decreasing the likelihood of strong stress buildup. Furthermore, extrapolation of the Slab2 model indicates that the slab depth at the location of lakes Castor and Pollux is around 140 km (Hayes et al., 2018), requiring minimum a ~M7 earthquake to cause shaking intensities of ≥VI½ (needed to trigger subaquatic mass-movements) based on an evaluation of historical Chilean events studied by Astroza et al. (2005) and global intraslab earthquakes at a similar depth (USGS, 2023). Considering that a rupture to produce such M7 earthquake should be at least 50 km in length (Wells and Coppersmith, 1994), combined with the short distance to the slab window, an intraslab source is deemed unlikely in this area.

5.4 Earthquake hazard in the Coyhaique region

Even though a future, similar relatively high-magnitude crustal event poses a serious hazard to the region, these events do not seem to occur frequently. The sedimentary infill of Lago Castor and Lago Pollux do not reveal any other similar, large-scale mass-wasting events throughout the Holocene, and there are no other traces of similar catchment responses in the sediment core from Aysén Fjord. Only a few MTDs in the middle of Unit 5.2 in Lago Pollux that are likely synchronous with a turbidite in Lago Castor (Van Daele et al., 2016) point to a similar event around 13 kyrs BP. However, as this is beyond the maximum age of the Aysén record, the sedimentary evidence is spatially insufficiently distributed to obtain meaningful modelling results. Hence, the local faults near Coyhaique do not seem to be very active, or do not produce sufficient shaking to be recorded in lake sediments. Indeed, several of the faults are too short to produce M>6.5 earthquakes which would cause strong shaking in a large area (Figure 10d). Furthermore, on the Lago Castor seismic profiles that cross the Castor Fault, we did not observe fault offset within Unit 5. This earthquake probability is in contrast to the LOFZ faults, for which 5 events, including the 2007

https://doi.org/10.5194/egusphere-2024-8
Preprint. Discussion started: 20 February 2024

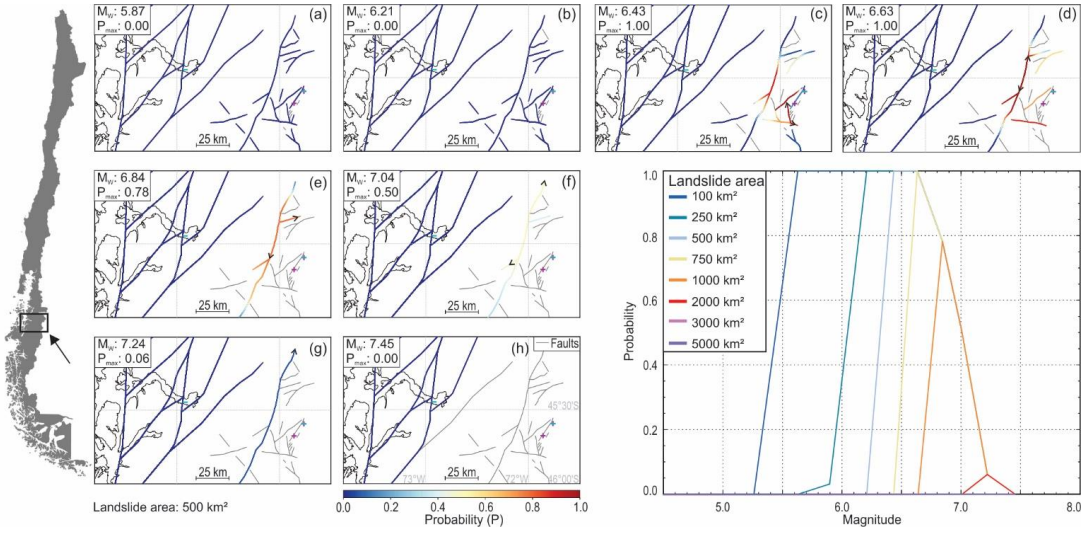

Figure 10. **Top left:** **Maps (location indicated on grey map of Chile) showing all faults in the study area, color-coded according to the probability that an earthquake of magnitude 5.87 (a), 6.21 (b), 6.43 (c), 6.63 (d), 6.84 (e), 7.04 (f), 7.24 (g) or 7.45 (h) on each of the fault sections is capable of causing the observed spatial distribution of sedimentary earthquake evidence and by considering an area of 500 km² that has been affected by landslides. Arrows indicate the limits of the rupture trace resulting in the highest probability. Grey fault traces are not sufficiently long to cause a rupture with the tested magnitude. Sites of positive (plus) and negative (minus) evidence are shown in semitransparent magenta and cyan colors, respectively. Note that sites with both positive and negative evidence show a bluish color.** **Bottom right:** **The maximum probability of an earthquake on any of the faults in the study area with a magnitude ranging between 5 and 7.6 to have caused the observed pattern of sedimentological imprints In Lago Pollux, Lago Castor and Aysén Fjord (positive and negative evidence), considering a range of minimum areas (100-5000 km²) in the Rio Aysén catchment that were affected by landslides.**

earthquake, have been identified throughout the Holocene (Wils et al., 2018). All of these events produced major mass-wasting in Aysén Fjord, and are the result of moderate-magnitude earthquakes on either of the LOFZ fault branches in the vicinity of the fjord (Vanneste et al., 2018). An additional event recently identified in Laguna Esponja around 166 CE (63 BC – 345 AD; Fagel et al., 2023) is potentially also related to activity of the LOFZ. Around this time, a coarse-grained turbidite has also been identified in the sedimentary infill of Aysén Fjord (youngest EM3 in Wils et al., 2020; 170 – 350 AD; note that our hypothesized correlation is different to that proposed by Fagel et al., 2023), potentially associated to onshore mass-wasting as well – albeit less pronounced compared to the aforementioned events (Wils et al., 2020). If these deposits indeed correlate, this would indicate the presence of a 6th event along the LOFZ, merely a few tens of years following one of the predecessors of the 2007 M_W 6.2 event (Wils et al., 2018).

6 Conclusions

Analysis of seismic reflection profiles of Lago Pollux reveals its sedimentary history and allows for a correlation with neighboring Lago Castor. Based on the published age depth models of Lago Castor and Aysén Fjord, a correlation between these three records was established. This correlation shows that synchronous mass-wasting occurred around ~4400 cal yrs BP in both lakes, while Aysén Fjord was not directly affected by subaqueous landslides but did experience the sedimentary effects of a ~50 years long catchment response as a result of major onshore mass-wasting in its catchment. Evidence for this catchment response was obtained by multiproxy analysis of a section in a sediment core retrieved from inner Aysén Fjord. Grain-size results showed that a portion, seen as a lighter-colored layer, showed a distinct finer-grained component. Furthermore, a lower organic matter content was found in this deposit, matching the already organic-poor andosol soils in the catchment area. Ground-motion modelling provides constraints on the location and magnitude of the triggering earthquake. For an affected area between 100 and 1000 km², an earthquake rupture along a local fault, with a magnitude range of 5.6-6.8 and intense shaking, is the most-likely scenario. A megathrust-related source mechanism or a rupture along the LOFZ as source could be

https://doi.org/10.5194/egusphere-2024-8
Preprint. Discussion started: 20 February 2024

ruled out. It can thus be concluded that the seismic hazard in the Aysén Region is not only restricted to the main, large-scale tectonic structures, but could also come from smaller local faults in the area. Further paleoseismic studies in small Patagonian lakes could aid in understanding the seismic hazard of these local faults.

Author contribution

Reflection-seismic interpretations of Lago Pollux and sedimentological analysis of the Aysén Fjord sediment core were carried out by Morgan Vervoort, aided by Maarten Van Daele and Katleen Wils. The Aysén Fjord sediment core was retrieved during a cruise for which C. Kissel was chief scientist. Analysis of the short cores in Lago Pollux and Lago Castor was carried out by Clara Paesbrugge, aided by Maarten Van Daele. Earthquake modelling was performed by Katleen Wils, applying a code developed by Kris Vanneste and Katleen Wils. Morgan Vervoort prepared the manuscript, with contributions from all co-authors.

Acknowledgements

This research was funded by the Research Foundation Flanders (FWO-Vlaanderen CHILT project) (FWO G.0778.09). K. Wils is funded by the Research Foundation – Flanders (FWO), grant 12ZC422N. We thank K. De Rycker, A. Peña and O. Wuendrich for invaluable, technical help on the field. We thank C. Paesbrugge for the sedimentological analysis of the Lago Castor and Lago Pollux short cores. We further thank the Isotope Bioscience Laboratory (ISOFYS) of Ghent University for the organic geochemical analysis.

References

Adams, J.: Paleoseismicity of the Cascadia Subduction Zone: Evidence from turbidites off the Oregon-Washington Margin, Tectonics, 9, 569–583, https://doi.org/10.1029/TC009i004p00569, 1990.

Agurto, H., Rietbrock, A., Barrientos, S., Bataille, K., and Legrand, D.: Seismo-tectonic structure of the Aysén Region, Southern Chile, inferred from the 2007 Mw= 6.2 Aysén earthquake sequence, Geophys J Int, 190, 116–130, https://doi.org/10.1111/j.1365-246X.2012.05507.x, 2012.

Astroza, M., Sandoval, M., and Kausel, E.: Estudio comparativo de los effectos de los sismos Chilenos de subducción del tipo intraplaca de profundidad intermedia., in: Congreso Chileno de Sismología e ingeniaría Antisísmica, 2005.

Avşar, U., Hubert-Ferrari, A., Batist, M. De, and Fagel, N.: A 3400 year lacustrine paleoseismic record from the North Anatolian Fault, Turkey: Implications for bimodal recurrence behavior, Geophys Res Lett, 41, 377–384, https://doi.org/10.1002/2013GL058221, 2014.

Bakun, W. H. and Wentworth, C. M.: Estimating Earthquake Location and Magnitude from Seismic Intensity Data, Bulletin of the Seismological Society of America, 87, 1502–1521, 1997.

Bernhardt, A., Melnick, D., Hebbeln, D., Lückge, A., and Strecker, M. R.: Turbidite paleoseismology along the active continental margin of Chile – Feasible or not?, Quat Sci Rev, 120, 71–92, https://doi.org/10.1016/j.quascirev.2015.04.001, 2015.

Carneiro, L. M., do Rosário Zucchi, M., de Jesus, T. B., da Silva Júnior, J. B., and Hadlich, G. M.: δ13C, δ15N and TOC/TN as indicators of the origin of organic matter in sediment samples from the estuary of a tropical river, Mar Pollut Bull, 172, https://doi.org/10.1016/j.marpolbul.2021.112857, 2021.

Cembrano, J. and Lara, L.: The link between volcanism and tectonics in the southern volcanic zone of the Chilean Andes: A review, Tectonophysics, 471, 96–113, https://doi.org/10.1016/j.tecto.2009.02.038, 2009.

https://doi.org/10.5194/egusphere-2024-8
Preprint. Discussion started: 20 February 2024

Cembrano, J., Lara, L., Lavenu, A., and Hervé, F.: Long-term and short-term kinematic history of the Liquiñe Ofqui fault zone, southern Chile: a review and implications for geologic hazard assessment, in: Proceedings Geological Society of America Annual Meeting, 2007.

Davies, B. J., Darvill, C. M., Lovell, H., Bendle, J. M., Dowdeswell, J. A., Fabel, D., García, J. L., Geiger, A., Glasser, N. F., Gheorghiu, D. M., Harrison, S., Hein, A. S., Kaplan, M. R., Martin, J. R. V., Mendelova, M., Palmer, A., Pelto, M., Rodés, Á., Sagredo, E. A., Smedley, R. K., Smellie, J. L., and Thorndycraft, V. R.: The evolution of the Patagonian Ice Sheet from 35 ka to the present day (PATICE), Earth Sci Rev, 204, 77, https://doi.org/10.1016/j.earscirev.2020.103152, 2020.

De La Cruz, R., Suárez, M., Belmar, M., Quiroz, D., and Bell, M.: Area Coihaique-Balmaceda, Region Aisen del General Carlos Ibañez del Campo, Carta Geologica de Chile, Servicio Nacional de Geologica Y Mineria, 2003.

Del Grosso, V. A.: New equation for the speed of sound in natural waters (with comparisons to other equations), Journal of the Acoustic Society of America, 56, 1084–1091, 1974.

Ellies, A.: Soil erosion and its control in Chile - An overview, Acta Geologica Hispanica, 35, 279–284, 2000.

Fagel, N., Pedreros, P., Alvarez, D., Israde Alcantara, I., Vega Alay, I., Namur, O., Araneda, A., Schmidt, S., Lepoint, G., and Urrutia, R.: Volcanic, tectonic and climate controls on lacustrine sedimentary supplies over the last millenia in NE Chilean Patagonia (Lake Esponja, Aysen, 45°S), Holocene, 33, 518–535, https://doi.org/10.1177/09596836231151828, 2023.

Gilli, A., Ariztegui, D., Anselmetti, F. S., McKenzie, J. A., Markgraf, V., Hajdas, I., and McCulloch, R. D.: Mid-Holocene strengthening of the Southern Westerlies in South America - Sedimentological evidences from Lago Cardiel, Argentina (49°S), Glob Planet Change, 49, 75–93, https://doi.org/10.1016/j.gloplacha.2005.05.004, 2005.

Gut, B.: Geology, climate and soils of Patagonia, in: Trees in Patagonia, Birkhäuser, Basel, 9–18, 2008.

Hayes, G. P., Moore, G. L., Portner, D. E., Hearne, M., Flamme, H., Furtney, M., and Smoczyk, G. M.: Slab2, a comprehensive subduction zone geometry model, Science (1979), 362, 58–61, https://doi.org/10.1126/science.aat4723, 2018.

Heirman, K., De Batist, M., Charlet, F., Moernaut, J., Chapron, E., Brümmer, R., Pino, M., and Urrutia, R.: Detailed seismic stratigraphy of Lago Puyehue: Implications for the mode and timing of glacier retreat in the Chilean Lake District, J Quat Sci, 26, 665–674, https://doi.org/10.1002/jqs.1491, 2011.

Heirman, K., De Batist, M., Arnaud, F., and De Beaulieu, J. L.: Seismic stratigraphy of the late Quaternary sedimentary infill of Lac d'Armor (Kerguelen archipelago): A record of glacier retreat, sedimentary mass wasting and southern Westerly intensification, Antarct Sci, 24, 608–618, https://doi.org/10.1017/S0954102012000466, 2012.

Henry, J. A.: Humid Climates, in: Encyclopedia of World Climatology, Springer Netherlands, 412–413, https://doi.org/10.1007/1-4020-3266-8_101, 2005.

Hervé, M. A.: Estudio geológico de la Falla Liquiñe-Reloncaví en el área de Liquiñe: Antecedentes de un movimiento transcurrente (Provincia de Valdivia), in: Primer Congreso Geologico Chileno, 1976.

Howarth, J. D., Fitzsimons, S. J., Norris, R. J., and Jacobsen, G. E.: Lake sediments record cycles of sediment flux driven by large earthquakes on the Alpine fault, New Zealand, Geology, 40, 1091–1094, https://doi.org/10.1130/G33486.1, 2012.

Howarth, J. D., Fitzsimons, S. J., Norris, R. J., and Jacobsen, G. E.: Lake sediments record high intensity shaking that provides insight into the location and rupture length of large earthquakes on the Alpine Fault, New Zealand, Earth Planet Sci Lett, 403, 340–351, https://doi.org/10.1016/j.epsl.2014.07.008, 2014.

Keefer, D. K.: Landslides caused by earthquakes, Bulletin of the Geological Society of America, 95, 406–421, https://doi.org/10.1130/0016-7606(1984)95<406:lcbe>2.0.co;2, 1984.

Kremer, K., Wirth, S. B., Reusch, A., Fäh, D., Bellwald, B., Anselmetti, F. S., Girardclos, S., and Strasser, M.: Lake-sediment based paleoseismology: Limitations and perspectives from the Swiss Alps, Quat Sci Rev, 168, 1–18, https://doi.org/10.1016/j.quascirev.2017.04.026, 2017.

Lazo, R. G.: Estudio de low daños de los terremotos del 21 y 22 de mayo de 1960, Universidad de Chile, Santiago, 2008.

https://doi.org/10.5194/egusphere-2024-8
Preprint. Discussion started: 20 February 2024

Legrand, D., Barrientos, S., Bataille, K., Cembrano, J., and Pavez, A.: The fluid-driven tectonic swarm of Aysen Fjord, Chile (2007) associated with two earthquakes (Mw=6.1 and Mw=6.2) within the Liquiñe-Ofqui Fault Zone, Cont Shelf Res, 31, 154–161, https://doi.org/10.1016/j.csr.2010.05.008, 2011.

Markgraf, V., Whitlock, C., and Haberle, S.: Vegetation and fire history during the last 18,000 cal yr B.P. in Southern Patagonia: Mallín Pollux, Coyhaique, Province Aisén (45°41′30″ S, 71°50′30″ W, 640 m elevation), Palaeogeogr Palaeoclimatol Palaeoecol, 254, 492–507, https://doi.org/10.1016/j.palaeo.2007.07.008, 2007.

Métois, M., Socquet, A., and Vigny, C.: Interseismic coupling, segmentation and mechanical behavior of the central Chile subduction zone, J Geophys Res Solid Earth, 117, 16, https://doi.org/10.1029/2011JB008736, 2012.

Meyers, P. A. and Ishiwatari, R.: Lacustrine organic geochemistryman overview of indicators of organic matter sources and diagenesis in lake sediments, Org Geochem, 20, 867–900, 1993.

Moernaut, J.: Time-dependent recurrence of strong earthquake shaking near plate boundaries: A lake sediment perspective, Earth Sci Rev, 103344, https://doi.org/10.1016/j.earscirev.2020.103344, 2020.

Moernaut, J. and De Batist, M.: Frontal emplacement and mobility of sublacustrine landslides: Results from morphometric and seismostratigraphic analysis, Mar Geol, 285, 29–45, 2011.

Moernaut, J., De Batist, M., Charlet, F., Heirman, K., Chapron, E., Pino, M., Brümmer, R., and Urrutia, R.: Giant earthquakes in South-Central Chile revealed by Holocene mass-wasting events in Lake Puyehue, Sediment Geol, 195, 239–256, https://doi.org/10.1016/j.sedgeo.2006.08.005, 2007.

Moernaut, J., Van Daele, M., Heirman, K., Fontijn, K., Strasser, M., Pino, M., Urrutia, R., and De Batist, M.: Lacustrine turbidites as a tool for quantitative earthquake reconstruction: New evidence for a variable rupture mode in south central Chile, J Geophys Res Solid Earth, 119, 1607–1633, https://doi.org/10.1002/2013JB010738, 2014.

Molenaar, A., Moernaut, J., Wiemer, G., Dubois, N., and Strasser, M.: Earthquake Impact on Active Margins: Tracing Surficial Remobilization and Seismic Strengthening in a Slope Sedimentary Sequence, Geophys Res Lett, 46, 6015–6023, https://doi.org/10.1029/2019GL082350, 2019.

Monecke, K., Anselmetti, F. S., Becker, A., Sturm, M., and Giardini, D.: The record of historic earthquakes in lake sediments of Central Switzerland, Tectonophysics, 394, 21–40, https://doi.org/10.1016/j.tecto.2004.07.053, 2004.

Moreno, P. I., Simi, E., Villa-Martínez, R. P., and Vilanova, I.: Early arboreal colonization, postglacial resilience of deciduous Nothofagus forests, and the Southern Westerly Wind influence in central-east Andean Patagonia, Quat Sci Rev, 218, 61–74, https://doi.org/10.1016/j.quascirev.2019.06.004, 2019.

Naranjo, J. A. and Stern, C. R.: Holocene explosive activity of Hudson Volcano, southern Andes, Bull Volcanol, 59, 291–306, https://doi.org/10.1007/s004450050193, 1998.

Naranjo, J. A. and Stern, C. R.: Holocene tephrochronology of the southernmost part (42°30'-45°8) of the Andean Southern Volcanic Zone, Revista Geológica de Chile, 31, 225–240, https://doi.org/10.4067/S0716-02082004000200003, 2004.

Naranjo, J. A., Arenas, M., Clavero, J., and Muñoz, O.: Mass movement-induced tsunamis: Main effects during the Patagonian Fjordland seismic crisis in Aisén (45°25'S), Chile, Andean Geology, 36, 137–145, https://doi.org/10.4067/s0718-71062009000100011, 2009.

Ndiaye, M., Clerc, N., Gorin, G., Girardclos, S., and Fiore, J.: Lake Neuchâtel (Switzerland) seismic stratigraphic record points to the simultaneous Würmian deglaciation of the Rhône Glacier and Jura Ice Cap, Quat Sci Rev, 85, 1–19, https://doi.org/10.1016/j.quascirev.2013.11.017, 2014.

Paterson, G. A. and Heslop, D.: New methods for unmixing sediment grain size data, Geochemistry, Geophysics, Geosystems, 16, 4494–4506, https://doi.org/10.1002/2015GC006070, 2015.

Piret, L., Bertrand, S., Kissel, C., De Pol-Holz, R., Tamayo Hernando, A., and Van^Daele, M.: First evidence of a mid-Holocene earthquake-triggered megaturbidite south of the Chile Triple Junction, Sediment Geol, 375, 120–133, https://doi.org/10.1016/j.sedgeo.2018.01.002, 2018.

Praet, N., Moernaut, J., Van Daele, M., Boes, E., Haeussler, P. J., Strupler, M., Schmidt, S., Loso, M. G., and De Batist, M.: Paleoseismic potential of sublacustrine landslide records in a high-seismicity setting (south-central Alaska), Mar Geol, 384, 103–119, https://doi.org/10.1016/j.margeo.2016.05.004, 2017.

Pribyl, D. W.: A critical review of the conventional SOC to SOM conversion factor, Geoderma, 156, 75–83, https://doi.org/10.1016/j.geoderma.2010.02.003, 2010.

Rein, B. and Sirocko, F.: In-situ reflectance spectroscopy - analysing techniques for high-resolution pigment logging in sediment cores, International Journal of Earth Sciences, 91, 950–954, https://doi.org/10.1007/s00531-002-0264-0, 2002.

Rodríguez, C. E., Bommer, J. J., and Chandler, R. J.: Earthquake-induced landslides: 1980–1997, Soil Dynamics and Earthquake Engineering, 18, 325–346, https://doi.org/10.1016/S0267-7261(99)00012-3, 1999.

Russo, R. M., VanDecar, J. C., Comte, D., Mocanu, V. I., Gallego, A., and Murdie, R. E.: Subduction of the Chile Ridge: Upper mantle structure and flow, GSA Today, 20, 4–10, https://doi.org/10.1130/GSATG61A.1, 2010.

Sabatier, P., Moernaut, J., Bertrand, S., Van Daele, M., Kremer, K., Chaumillon, E., and Arnaud, F.: A Review of Event Deposits in Lake Sediments, Quaternary, 5, https://doi.org/10.3390/quat5030034, 2022.

Schnellmann, M., Anselmetti, F. S., Giardini, D., Mckenzie, J. A., and Ward, S. N.: Prehistoric earthquake history revealed by lacustrine slump deposits, Geology, 30, 1131–1134, 2002.

Sepúlveda, S. A., Serey, A., Lara, M., Pavez, A., and Rebolledo, S.: Landslides induced by the April 2007 Aysén Fjord earthquake, Chilean Patagonia, Landslides, 7, 483–492, https://doi.org/10.1007/s10346-010-0203-2, 2010.

Sernageomin: Mapa geologico de Chile: version digital, Servicio Nacional de Geologia y Mineria, Santiago, 2003.

Serva, L., Vittori, E., Comerci, V., Esposito, E., Guerrieri, L., Michetti, A. M., Mohammadioun, B., Mohammadioun, G. C., Porfido, S., and Tatevossian, R. E.: Earthquake Hazard and the Environmental Seismic Intensity (ESI) Scale, in: Pure and Applied Geophysics, vol. 173, 1479–1515, https://doi.org/10.1007/s00024-015-1177-8, 2016.

Shanahan, T. M., McKay, N., Overpeck, J. T., Peck, J. A., Scholz, C., Heil, C. W., and King, J.: Spatial and temporal variability in sedimentological and geochemical properties of sediments from an anoxic crater lake in West Africa: Implications for paleoenvironmental reconstructions, Palaeogeogr Palaeoclimatol Palaeoecol, 374, 96–109, https://doi.org/10.1016/j.palaeo.2013.01.008, 2013.

Stern, C. R.: Active Andean volcanism: its geologic and tectonic setting, Revista Geológica de Chile, 31, 161–206, https://doi.org/10.4067/S0716-02082004000200001, 2004.

St.-Onge, G., Mulder, T., Piper, D. J. W., Hillaire-Marcel, C., and Stoner, J. S.: Earthquake and flood-induced turbidites in the Saguenay Fjord (Québec): A Holocene paleoseismicity record, Quat Sci Rev, 23, 283–294, https://doi.org/10.1016/j.quascirev.2003.03.001, 2004.

Strasser, M., Stegmann, S., Bussmann, F., Anselmetti, F. S., Rick, B., and Kopf, A.: Quantifying subaqueous slope stability during seismic shaking: Lake Lucerne as model for ocean margins, Mar Geol, 240, 77–97, https://doi.org/10.1016/j.margeo.2007.02.016, 2007.

Thomson, S. N.: Late Cenozoic geomorphic and tectonic evolution of the Patagonian Andes between latitudes 42S and 46S: An appraisal based on fission-track results from the transpressional intra-arc Liquiñe-Ofqui fault zone, GSA Bulletin, 114, 1159–1173, 2002.

Trachsel, M., Grosjean, M., Schnyder, D., Kamenik, C., and Rein, B.: Scanning reflectance spectroscopy (380-730 nm): A novel method for quantitative high-resolution climate reconstructions from minerogenic lake sediments, J Paleolimnol, 44, 979–994, https://doi.org/10.1007/s10933-010-9468-7, 2010.

Earthquake Hazards Program - Search Earthquake Catalog: https://earthquake.usgs.gov/earthquakes/search/, last access: 22 September 2023.

Van Daele, M., Moernaut, J., Doom, L., Boes, E., Fontijn, K., Heirman, K., Vandoorne, W., Hebbeln, D., Pino, M., Urrutia, R., Brümmer, R., and De Batist, M.: A comparison of the sedimentary records of the 1960 and 2010 great Chilean earthquakes

https://doi.org/10.5194/egusphere-2024-8
Preprint. Discussion started: 20 February 2024

in 17 lakes: Implications for quantitative lacustrine palaeoseismology, Sedimentology, 62, 1466–1496, https://doi.org/10.1111/sed.12193, 2015.

Van Daele, M., Bertrand, S., Meyer, I., Moernaut, J., Vandoorne, W., Siani, G., Tanghe, N., Ghazoui, Z., Pino, M., Urrutia, R., and De Batist, M.: Late Quaternary evolution of Lago Castor (Chile, 45.6°S): Timing of the deglaciation in northern Patagonia and evolution of the southern westerlies during the last 17 kyr, Quat Sci Rev, 133, 130–146, https://doi.org/10.1016/j.quascirev.2015.12.021, 2016.

Van Daele, M., Araya-Cornejo, C., Pille, T., Vanneste, K., Moernaut, J., Schmidt, S., Kempf, P., Meyer, I., and Cisternas, M.: Distinguishing intraplate from megathrust earthquakes using lacustrine turbidites, Geology, 47, 127–130, https://doi.org/10.1130/G45662.1, 2019.

Van Daele, M., Haeussler, P. J., Witter, R. C., Praet, N., and De Batist, M.: The Sedimentary Record of the 2018 Anchorage Earthquake in Eklutna Lake, Alaska: Calibrating the Lacustrine Seismograph, Seismological Research Letters, 91, 126–141, https://doi.org/10.1785/0220190204, 2020.

Vandekerkhove, E., Van Daele, M., Praet, N., Cnudde, V., Haeussler, P. J., and De Batist, M.: Flood-triggered versus earthquake-triggered turbidites: A sedimentological study in clastic lake sediments (Eklutna Lake, Alaska), Sedimentology, 67, 364–389, https://doi.org/10.1111/sed.12646, 2020.

Vanneste, K., Wils, K., and Van Daele, M.: Probabilistic Evaluation of Fault Sources Based on Paleoseismic Evidence From Mass-Transport Deposits: The Example of Aysén Fjord, Chile, J Geophys Res Solid Earth, 123, 9842–9865, https://doi.org/10.1029/2018JB016289, 2018.

Van Rensbergen, P., De Batist, M., Beck, Ch., and Manalt, F.: High-resolution seismic stratigraphy of late Quaternary fill of Lake Annecy (northwestern Alps): evolution from glacial to interglacial sedimentary processes, Sediment Geol, 117, 71–96, 1998.

Weller, D., Miranda, C. G., Moreno, P. I., Villa-Martínez, R., and Stern, C. R.: The large late-glacial Ho eruption of the Hudson Volcano, southern Chile, Bull Volcanol, 76, https://doi.org/10.1007/s00445-014-0831-9, 2014.

Weller, D. J., De Porras, M. E., Maldonado, A., Méndez, C., and Stern, C. R.: New age controls on the tephrochronology of the southernmost Andean Southern Volcanic Zone, Chile, Quat Res, 1–15, https://doi.org/10.1017/qua.2018.81, 2018.

Wells, D. and Coppersmith, K. J.: New empirical relationships among magnitude, rupture length, rupture width, rupture area, and surface displacement, Bulletin of the Seismological Society of America, 84, 974–1002, 1994.

Wilhelm, B., Nomade, J., Crouzet, C., Litty, C., Sabatier, P., Belle, S., Rolland, Y., Revel, M., Courboulex, F., Arnaud, F., and Anselmetti, F. S.: Quantified sensitivity of small lake sediments to record historic earthquakes: Implications for paleoseismology, J Geophys Res Earth Surf, 121, 2–16, https://doi.org/10.1002/2015JF003644, 2016.

Wils, K., Van Daele, M., Lastras, G., Kissel, C., Lamy, F., and Siani, G.: Holocene Event Record of Aysén Fjord (Chilean Patagonia): An Interplay of Volcanic Eruptions and Crustal and Megathrust Earthquakes, J Geophys Res Solid Earth, 123, 324–343, https://doi.org/10.1002/2017JB014573, 2018.

Wils, K., Van Daele, M., Kissel, C., Moernaut, J., Schmidt, S., Siani, G., and Lastras, G.: Seismo-Turbidites in Aysén Fjord (Southern Chile) Reveal a Complex Pattern of Rupture Modes Along the 1960 Megathrust Earthquake Segment, J Geophys Res Solid Earth, 125, 1–23, https://doi.org/10.1029/2020JB019405, 2020.